



**HAL**  
open science

## Synergy between the Host Immune System and Bacteriophage Is Essential for Successful Phage Therapy against an Acute Respiratory Pathogen

Dwayne Roach, Chung Yin Leung, Marine Henry, Eric Morello, Devika Singh, James P Di Santo, Joshua Weitz, Laurent Debarbieux

► **To cite this version:**

Dwayne Roach, Chung Yin Leung, Marine Henry, Eric Morello, Devika Singh, et al.. Synergy between the Host Immune System and Bacteriophage Is Essential for Successful Phage Therapy against an Acute Respiratory Pathogen. *Cell Host and Microbe*, 2017, 22 (1), pp.38 - 47.e4. 10.1016/j.chom.2017.06.018 . pasteur-01827320

**HAL Id: pasteur-01827320**

**<https://pasteur.hal.science/pasteur-01827320>**

Submitted on 19 Jul 2018

**HAL** is a multi-disciplinary open access archive for the deposit and dissemination of scientific research documents, whether they are published or not. The documents may come from teaching and research institutions in France or abroad, or from public or private research centers.

L'archive ouverte pluridisciplinaire **HAL**, est destinée au dépôt et à la diffusion de documents scientifiques de niveau recherche, publiés ou non, émanant des établissements d'enseignement et de recherche français ou étrangers, des laboratoires publics ou privés.

1 **Title**

2 **Synergy between the host immune system and bacteriophage is**  
3 **essential for successful phage therapy against an acute respiratory**  
4 **pathogen**

5

6

7 **Authors**

8 Dwayne R. Roach<sup>1\*</sup>, Chung Yin Leung<sup>2,3\*</sup>, Marine Henry<sup>1</sup>, Eric Morello<sup>1</sup>, Devika Singh<sup>2</sup>, James  
9 P. Di Santo<sup>4,5</sup>, Joshua S. Weitz<sup>2,3#</sup>, and Laurent Debarbieux<sup>1#§</sup>

10

11 **Affiliations**

12 <sup>1</sup>Department of Microbiology, Institut Pasteur, Paris 75015, FR

13 <sup>2</sup>School of Biological Sciences, Georgia Institute of Technology, Atlanta, Georgia 30332, USA

14 <sup>3</sup>School of Physics, Georgia Institute of Technology, Atlanta, Georgia 30332, USA

15 <sup>4</sup>Innate Immunity Unit, Department of Immunology, Institut Pasteur, Paris 75015, FR

16 <sup>5</sup>Inserm U1223, Paris 75015, FR

17

18 \*These authors contributed equally to this work.

19 §Lead contact email: laurent.debarbieux@pasteur.fr

20 #Corresponding author email: laurent.debarbieux@pasteur.fr & jsweitz@gatech.edu

21

22

23 **Summary:**

24 The rise of multi-drug resistant (MDR) bacteria has spurred renewed interest in the use of  
25 bacteriophages as therapy. However, mechanisms underlying contributing to phage-mediated  
26 bacterial clearance in an animal host remain unclear. We investigated the effects of host  
27 immunity on the efficacy of phage therapy for acute pneumonia caused by MDR *Pseudomonas*  
28 *aeruginosa* in a mouse model. Comparing efficacies of phage curative and prophylactic  
29 treatments in healthy immunocompetent, MyD88 deficient, lymphocyte deficient, and neutrophil  
30 depleted murine hosts, revealed that neutrophil-phage synergy is essential for the resolution of  
31 pneumonia. Population modeling of *in vivo* results further showed that neutrophils are required  
32 to control both phage-sensitive and emergent phage-resistant variants to clear infection. This  
33 ‘immunophage synergy’ contrasts with the paradigm that phage therapy success is largely due to  
34 bacterial permissiveness to phage killing. Lastly, therapeutic phages were not cleared by  
35 pulmonary immune effector cells, and were immunologically well tolerated by lung tissues.

36

37

38 **Introduction**

39 The global spread of antibiotic resistant bacteria threatens all aspects of modern medicine,  
40 including advances in treatment of infectious disease, surgery, transplantation, and chemotherapy  
41 (Brogan and Mossialos, 2016). An acutely worrying trend is the spread of resistance to  
42 carbapenems – the 'antibiotics of last resort' – predominantly among Gram-negative bacteria  
43 including *Pseudomonas aeruginosa*, *Klebsiella pneumoniae*, and *Escherichia coli* (Brogan and  
44 Mossialos, 2016; CDC, 2013; Murray et al., 2015). Carbapenem resistance is almost always  
45 associated with resistance to several other classes of antibiotics leading to the rise of multi-drug  
46 resistant (MDR) bacteria (Brogan and Mossialos, 2016; Murray et al., 2015). Of the MDR  
47 bacteria, *P. aeruginosa* is a nosocomial opportunistic pathogen critical to the differential  
48 diagnosis of many gram-negative infections, including pneumonia, bacteraemia, and urinary tract  
49 infections (CDC, 2013; Murray et al., 2015). Individuals with chronic pulmonary disorders, such  
50 as cystic fibrosis (CF), are also at considerable risk of *P. aeruginosa* respiratory infections  
51 (Salsgiver et al., 2016). With few, if any, replacements for  $\beta$ -lactam antibiotics in development,  
52 especially the carbapenems, physicians and scientists have renewed efforts to identify alternative  
53 antibacterial therapies (Czaplewski et al., 2016).

54

55 Phage therapy is an antibacterial approach that involves introducing bacterial viruses (phages)  
56 that infect and lyse bacteria to cure or prevent infectious disease (Knoll and Mylonakis, 2014;  
57 Roach and Debarbieux, 2017; Salmond and Fineran, 2015). In a growing era of precision  
58 medicine, phage therapy has the distinct advantage over broad-spectrum antibiotics of being  
59 highly specific towards target bacterial pathogens without adversely affecting the host or host  
60 commensal microbiota (Sarker et al., 2016a). Pre-clinical animal studies have also shown

61 success rates of phage therapy up to 100% for curing infections caused by MDR pathogens,  
62 including *P. aeruginosa* (Debarbieux et al., 2010; Pabary et al., 2016). Furthermore, a limited  
63 number of clinical trials evaluating phage therapy in humans have shown promising results  
64 (Abedon et al., 2011; Vandenheuvél et al., 2015). However, other clinical trials have produced  
65 conflicting results, e.g., demonstrating safety of phage but failing to provide evidence for  
66 improved clinical outcomes (Rhoads et al., 2009; Sarker et al., 2016b). These data suggest the  
67 need to investigate the basis for therapeutic effectiveness, e.g., when and how is phage therapy  
68 effective, who should receive phage therapy, and how will phages be immunologically tolerated?  
69

70 A mechanistic understanding of phage therapy and the inherent tension between clinical aims  
71 and the biological processes underlying phage-bacteria dynamics has yet to be resolved. Phages  
72 are obligate intracellular parasites and the frequency of phage infection decreases with  
73 decreasing target host abundance (Adams, 1959). Consequently, therapeutic phage populations  
74 may reach a dynamic equilibrium with a target bacterial host population rather than eradicating it  
75 (Campbell, 1961; Levin et al., 1977; Weitz, 2015). In addition, *in vitro* studies have shown that  
76 exposure to high densities of phage often selects for phage-resistant bacteria (Luria and  
77 Delbrück, 1943), which can lead to the elimination of administered therapeutic phages  
78 (Dennehy, 2012; Meyer et al., 2012). The emergence of phage resistance represents a major  
79 conceptual and practical problem in moving from *in vitro* studies to the development of clinical  
80 phage therapy.

81  
82 In a therapeutic setting, phage-bacteria dynamics unfold in tandem with pressures from the  
83 mammalian host immunity. Hence, host immune status will both influence susceptibility to

84 pathogen infection, as well as the effectiveness of antimicrobial therapeutic agents, such as  
85 phages. Mathematical models have previously explored the potential consequences of  
86 interactions among bacterial infection, phage killing, and host immunity (Levin and Bull, 1996;  
87 Levin and Bull, 2004). However, these mathematical models do not account for the self-  
88 limitation of healthy host immune responses that prevents excessive tissue damage. In addition,  
89 the models assume that host immune responses are unaffected by pathogen densities, whereas *in*  
90 *vivo* immune defenses have been shown to become saturated at high pathogen densities (Drusano  
91 et al., 2011). Together, such assumptions drive model predictions that hosts can eliminate  
92 infections without therapeutic intervention.

93

94 Building on the modeling work of Levin and Bull (2004), we recently proposed the incorporation  
95 of a maximum capacity and density-dependent saturation of host immune defenses (Leung and  
96 Weitz, 2016). With these additions, our proof-of-principle (PoP) *in silico* population model  
97 predicts that host immune defenses alone cannot eradicate infection at high bacterial burden.  
98 Furthermore, combining mathematical analysis and numerical simulation, our PoP model  
99 predicts that the added antibacterial activity of phages combined with the host's own immune  
100 defenses leads to asymptotic eradication of bacterial infections (Leung and Weitz, 2016).  
101 Although, our *in silico* model predicted that phage therapy effectiveness is not inevitable and  
102 dependent on active host immune defenses, it did not consider the proliferation of phage  
103 resistance.

104

105 *P. aeruginosa* is particularly well suited to investigate the interactions between phage, a bacterial  
106 pathogen, and the immune response in an animal model of phage therapy. This bacterium

107 predominately causes pneumonia in patients with weakened or deficient immune defenses, which  
108 may have drastic effects to the efficacy of respiratory phage therapy. To investigate the effect of  
109 different host immunological states on the efficacy of phage therapy, we combine *in vivo*  
110 experiments and *in silico* modeling of phage-treated acute pneumonia caused by MDR *P.*  
111 *aeruginosa*. Together, we demonstrate that acute respiratory infections can be cured and  
112 prevented with phage therapy, provided there is a synergy with host innate immunity, in  
113 particular with neutrophils. Phage therapy was also immunologically well tolerated by the hosts.

114

## 115 **Results**

### 116 ***In vivo* phage therapy of acute respiratory infection**

117 From previous work, the pseudomonas phage PAK\_P1 has been characterized as being a double  
118 stranded DNA virus belonging to the Myoviridae family with a strictly virulent (lytic) life-cycle  
119 (Debarbieux et al., 2010; Henry et al., 2015). Phage PAK\_P1 has been shown *in vitro* to be well  
120 suited for lysing *P. aeruginosa* strains isolated from acute exacerbations rather than those strains  
121 found to chronically infect cystic fibrosis lungs. In addition, we have demonstrated using *in vivo*  
122 imaging that phage PAK\_P1 can be an efficient cure for acute pneumonia caused by the MDR *P.*  
123 *aeruginosa* in mice (Debarbieux et al., 2010).

124

125 Here, we examine the efficacy of curative treatment of acute pneumonia in mice with innate  
126 and/or adaptive immunity deficiencies by quantifying the light emitted by the bioluminescent *P.*  
127 *aeruginosa* strain PAK in live mice (Fig. 1A). First, we demonstrated that a single inhaled phage  
128 PAK\_P1 dose at a multiplicity of infection (MOI) of 10 (i.e.  $10^8$  plaque forming units [PFU])  
129 delivered after a 2h delay rescued 100% of *P. aeruginosa* lung infected immunocompetent wild-

130 type mice (Fig 1B). By quantifying light emitted from the chest regions (Fig. 1C and S1), we  
131 could monitor the proliferation and decline of bacterial densities as a function of  
132 bioluminescence in each lung of live animals in real-time (Fig. S1) (Andreu et al., 2011;  
133 Debarbieux et al., 2010). Imaging showed that bacterial bioluminescence began to decrease in as  
134 little as 2h post treatment in immunocompetent animals and was no longer detectable after 48h.  
135 In contrast, bioluminescence increased unimpeded post infection to an bacterial density of  $\sim 2.4$   
136  $\times 10^9$  CFU/g of lung tissue (*in vivo* radiance of  $\sim 4.8 \times 10^4$  p/s/cm<sup>2</sup>/sr) at 24h post infection in  
137 PBS mock-treated control animals (Fig. 1C) (Debarbieux et al., 2010). Shortly thereafter mock-  
138 treated controls died (Fig. 1B). These experimental results provided as a baseline prognosis for  
139 comparison of *in vivo* and *in silico* modeling the effects of immunodeficiency on phage therapy  
140 efficacy.

141

#### 142 ***In silico* modeling of respiratory phage therapy**

143 We adapt our PoP population model (Fig 2A) developed previously (Leung and Weitz, 2016) to  
144 the phage treatment and infection challenge doses used in our *in vivo* acute pneumonia  
145 experiments (Table S1 and Eq. 1-3). Contrary to expectations, the initial *in silico* simulations of  
146 the PoP model predicted a highly-accelerated clearance of infection (<1h) (Fig. S2A), which is  
147 independent of host immunity and happens even in its absence (Fig. S2B). This rapid clearance  
148 timescale was inconsistent with our *in vivo* observations (Fig. 1C). We postulate that the  
149 inconsistency is due to overestimating phage lysis rates as a result of the assumption that phage  
150 and bacteria populations were ‘well-mixed’ *in vivo*. In a well-mixed environment, the phage lysis  
151 rate is expected to be proportional to phage population densities (Fig. S2C). Instead, we  
152 hypothesize that the rate of bacteria lysis *in vivo* increases sublinearly with increasing phage

153 densities.

154

155 We identified two potential mechanisms *in vivo* that could be responsible for a sublinear phage  
156 lysis rate: spatial heterogeneity and phage saturation. Anatomical barriers in the mouse  
157 respiratory track could reduce encounters between phage and bacteria populations (Florens et al.,  
158 2011; Weibel, 1963). We account for such spatial heterogeneity by introducing power-law  
159 density dependence to the phage lysis rate (Fig. S2D and Eq. 4), following the convention of  
160 spatial epidemiological models (Roy and Pascual, 2006). We termed this the Heterogeneous  
161 Mixing (*HM*) model. Simulations of the *HM* model predict that the combined host immunity and  
162 phage lysis lead to bacterial population elimination over a longer course of 24h (Fig. 2B), which  
163 is consistent with our *in vivo* results (Fig. 1C). Without phage treatment, bacterial growth would  
164 rapidly saturate the host immune response and reach fatal levels within 48h (Fig. S3). This was  
165 also consistent with our mock-treated *in vivo* measurements (Fig. 1C). Another potential cause of  
166 sublinear phage lysis rates is phage saturation. This occurs when multiple phages adsorb to the  
167 same target bacterial cell when at a high phage population density (Abedon, 2009; Brown and  
168 Bidle, 2014). Therefore, we developed a second population model, termed the Phage Saturation  
169 (*PS*) model, to alternatively account for phage saturation (Fig S2H and Eq. 5). Simulations of the  
170 *PS* model (Fig. 2C) were also consistent with *in vivo* bioluminescence outcomes (Fig. 1C), as  
171 well as yielded qualitatively equivalent results as simulations with the *HM* model (Fig. 2B).

172

173 The synergistic elimination of bacterial pathogens over relevant time-scales was a robust feature  
174 of both *in silico* models. To probe robustness, we systematically varied the nonlinear phage  
175 adsorption rate and power-law exponent for the *HM* model (Figs. S2E and S2F), while for the *PS*

176 model, we systematically varied the phage adsorption rate and phage density at half saturation  
177 (Figs. S2I and S2J). Both models yield a large region of synergistic clearance of bacteria, in  
178 which phage and host immunity can eradicate the bacterial population only when combined  
179 (Figs. S2G and S2K). Despite this qualitative agreement, there were some differences in the *in*  
180 *silico* predictions of these two models. For example, the *PS* model predicts a relatively lower  
181 maximum and faster elimination of bacterial burden in the lungs of immunocompetent hosts,  
182 when compared to the *HM* model. In addition, the *HM* model exhibited greater robustness of the  
183 synergistic clearance regime to changes in variation in lysis parameters over the range of  
184 parameter scenarios we investigated than did the *PS* model.

185

### 186 ***In silico* modeling of phage resistance**

187 Leveraging our findings of synergistic clearance in both the *HM* and *PS* models given a phage-  
188 susceptible population of pathogenic bacteria, we then investigated if the emergence of phage-  
189 resistant bacteria can lead to monophage (use of a single phage type) therapy failure (Fig. 2D).  
190 Both the *HM* and *PS* models were extended to include the outgrowth of phage-resistant bacterial  
191 mutants with a fixed probability per cellular division. We also applied a modest 10% trade-off  
192 between phage resistance and cellular growth rate of the mutants (Bohannon et al., 2002) (Table  
193 S1 and Fig. S2D). These extended models were termed the *HM-R* and *PS-R*, respectively (Eq. 6-  
194 9). Both the *HM-R* (Fig. 2E) and *PS-R* (Fig. 2F) models predicted similar curative outcomes in  
195 immunocompetent hosts despite the transient presence of phage-resistant bacteria. That is, phage  
196 lysis in both *HM-R* and *PS-R* models can initially decrease the phage-sensitive bacterial  
197 population giving way to phage-resistant mutant outgrowth. However, the phage-resistant  
198 bacteria are eliminated by host innate immunity. This suggests that asymptotic clearance of

199 infection requires the synergy of both phage lysis and innate immunity. We utilized both models  
200 to further investigate the effects of immunodeficiency on phage therapy, given their  
201 compatibility with initial *in vivo* experiments.

202

### 203 **Immune signaling deficiency allows for phage resistance outgrowth**

204 Invading bacteria encounter the hosts' first line innate immune defenses, e.g., neutrophils and  
205 innate lymphocytes that sense microbes via pathogen recognition receptors (PRRs), such as the  
206 Toll-like receptors (TLRs). When activated by ligand binding, TLRs induce several effector  
207 functions to contain and eradicate infectious threats. To provide insight into which immune  
208 component was responsible for immunity-phage synergism, we first evaluated phage therapy  
209 efficacy in hosts with Myeloid Differentiation factor 88 (MyD88) deficiency. MyD88 is a central  
210 signaling transduction protein for most ligand-activated TLRs eliciting both innate and adaptive  
211 immune responses (Warner and Nunez, 2013).

212

213 MyD88 deficiency has been shown to cause impaired innate immune responses toward *P.*  
214 *aeruginosa* (Skerrett et al., 2004). Here, we confirm that *MyD88*<sup>-/-</sup> mice are highly susceptible  
215 to *P. aeruginosa* respiratory infection compared to wild-type mice. An infectious inoculum of  
216 10<sup>7</sup> colony forming units (CFU) caused highly rapid mortality in *MyD88*<sup>-/-</sup> mice. Therefore, we  
217 reduced the infectious inoculum 100-fold to decrease the time to mortality (Fig. 3A). Despite a  
218 more modest clinical course, phage treatment only improved survival by 15% over PBS mock-  
219 treated controls (p= 0.0287). Notably, bioluminescence in the lungs of *Myd88*<sup>-/-</sup> mice showed  
220 that phage treatment significantly reduced bacterial burden to near undetectable levels by the 24h  
221 time point post infection (p.i.) compared to the mock-treated mice (p< 0.001) (Fig. 3B).

222 However, treatment failed to prevent fatality due to subsequent bacterial outgrowth after 24h.  
223 We surmise that the resurgent bacterial outgrowth was not due to a low abundance of phages in  
224 the lungs, since a reduction in bioluminescence implies sufficient phage replication occurred.  
225 Rather, we found that 100% of *P. aeruginosa* clones recovered from phage-treated *Myd88*<sup>-/-</sup>  
226 lungs at 24h p.i. were resistant to phage lysis with *in vitro* plaque analysis.

227

228 *In silico* modeling was used to determine if emergence of phage-resistant population in hosts that  
229 lack Myd88 immune activation would support phage treatment failure seen *in vivo*. Myd88  
230 deficiency has been shown to prevent immune cell activation and recruitment to the site of  
231 infection (Kawai et al., 1999; Warner and Nunez, 2013). In the models, we account for Myd88  
232 deficiency by maintaining immune response intensity at a basal level ( $I = I_0$ ) (Eq. 10). This still  
233 allows for marginal immune defenses during infection by the present immune effector cells in  
234 the lungs (Barletta et al., 2012). Without Myd88 immune signaling, both the *HM-R* (Fig. 3C) and  
235 *PS-R* (Fig. 3D) models predict that phage lysis will reduce phage-sensitive bacteria, with  
236 subsequent unimpeded outgrowth of phage-resistant mutants until mortality. Importantly, the  
237 predicted phage-resistant outgrowth rate was comparable to the regained bioluminescence seen  
238 after 24h with live imaging of *Myd88*<sup>-/-</sup> mice (Fig. 3B). We surmise that without immune  
239 activation, phage-resistant mutants overwhelm the basal immune defenses leading to a  
240 resurgence of the bacterial population that ultimately causes mortality.

241

242 In the clinic, patients can suffer from various degrees of weakened and deficient immunity.  
243 Building upon our initial results, we modeled *in silico* the effects of intermediate levels of  
244 immune activation on phage therapy efficacy by modifying the maximum immune response. The

245 maximum immune response is scaled such that at 0% immune activation, the immune response  
246 stays at the basal level, while at 100% immune activation the immune response can reach the  
247 maximum level in healthy individuals (Eq. 10). These simulations predicted that phage therapy  
248 will be effective and prevent outgrowth of emergent phage-resistant mutants provided immune  
249 activation exceeds 50% of that of a healthy immune response (Figs. 3E and S4A). However, our  
250 *in silico* models also predict that even without phage resistance, successful phage therapy still  
251 requires at least 20% immune responses to completely eradicate the phage-sensitive bacterial  
252 population in the lungs (Figs. S4B and S4C).

253

#### 254 **Null effect of lymphocyte deficiency for phage therapy**

255 As shown in figure 3, MyD88 signaling deficiency strongly reduced the efficacy of monophage  
256 treatment of *P. aeruginosa* respiratory infection. Next, we sought to explore which innate  
257 effector cell type(s) contribute to successful respiratory phage therapy in immunocompetent  
258 mice. MyD88 dependent TLR-activation triggers several immune pathways that together  
259 orchestrate innate immune responses while also initiating adaptive immunity (Warner and  
260 Nunez, 2013). Innate immune effector cells can be divided into numerous subsets, but are  
261 broadly categorized as being either from lymphoid or myeloid lineages. Innate lymphoid cells  
262 (ILCs) — including natural killer cells (NK cells) and recently discovered ILC1, ILC2 and ILC3  
263 — are enriched at mucosal surfaces and exert crucial defensive functions (Eberl et al., 2015).  
264 *Rag2<sup>-/-</sup>Il2rg<sup>-/-</sup>* mice carry a double germline knockout in recombination activating gene 2 and  
265 common gamma chain that prevent the production of ILCs, and antigen-specific T and B cells  
266 (Colucci et al., 1999). Here, we demonstrate that the same phage treatment dose ( $10^8$  PFU) used  
267 to cure acute pneumonia in immunocompetent mice, also rescued >90% of  $10^7$  CFU infected

268 *Rag2<sup>-/-</sup>Il2rg<sup>-/-</sup>* mice (Fig. 4A). Likewise, *in vivo* imaging revealed a qualitatively similar  
269 bioluminescence profile (Figs. 4B and S1) as phage-treated wild-type mice (Figs. 1C and S1). In  
270 *Rag<sup>-/-</sup>Il2rg<sup>-/-</sup>* mice, the lack of both innate and adaptive lymphoid cells does not seem to be a  
271 confounding factor for phage therapy of acute respiratory infection.

272

### 273 **Neutrophil–phage synergy is required for effective phage therapy**

274 Myeloid cells, including neutrophils, are major players for the innate inflammatory response to  
275 invading pathogens (Kolaczkowska and Kubes, 2013). We found that *P. aeruginosa* lung  
276 infected wild-type mice depleted of their neutrophils were completely unresponsive to inhaled  
277 phage treatment (Fig. 5A), even after reducing the bacterial challenge by 100-fold ( $10^5$  CFU) of  
278 that given to immunocompetent wild-type animals (Fig 1). Compared to Myd88 immune  
279 signaling deficient animals (Fig. 3B), phage treatment in neutrophil depleted hosts caused no  
280 significant reduction in bioluminescence after phage treatment (Fig. 5B).

281

282 Next, we probed the effect of neutrophil depletion on phage therapy using *in silico* modeling by  
283 setting host innate immunity to zero (Eq. 11). The *HM-R* math model predicts similar dynamical  
284 outcomes between severe neutropenia (Fig 5C) and that predicted for Myd88 deficient hosts  
285 (Fig. 3C). That is, the *HM-R* model predicts a significant reduction in bacterial density before  
286 phage-resistant outgrowth after 24h. However, this reduction was not seen *in vivo* (Fig. 5B). On  
287 the other hand, *PS-R* simulations of phage-treated neutrophil depleted hosts did not predict a  
288 significant reduction in the phage-sensitive bacteria, but rather a decline in their population  
289 growth rate before being replaced by phage-resistant outgrowth (Fig. 5D). This was more in line  
290 with *in vivo* observations, although the decline was not significantly different from mock-treated

291 animals (Fig. 5B). The *PS-R* model also predicts that host neutrophils are needed to  
292 synergistically eliminate the bacteria during phage therapy. Overall, *in vivo* experiments and both  
293 models suggest that phage therapy of acute respiratory disease may be inadequate for patients  
294 with severe neutropenia.

295  
296 Neutropenia encompasses a wide range of diagnoses from normal variants to life-threatening  
297 acquired (e.g. chemotherapy) and congenital disorders. It is generally defined as having blood  
298 neutrophil levels less than  $10^9/L$ , but the functional consequences is largely dependent on the  
299 severity of neutrophil depletion (Newburger and Dale, 2013). For instance, hosts with an  
300 estimated 12-23% absolute neutrophil count (ANC) of healthy levels, may only have a slightly  
301 increased risk of infection. However, ANCs below 5% (referred to as “agranulocytosis”) carries  
302 a high risk of severe infection (Newburger and Dale, 2013). We *in silico* modeled the effect of  
303 different neutrophil counts in the lungs on the efficacy of phage therapy (Eq. 11). Both the *PS-R*  
304 (Fig. 5E) and *HM-R* (Fig. S4D) models predict that successful phage therapy could be achieved  
305 with emergent phage resistance, provided at least 50% of healthy lung neutrophil counts were  
306 present. Moreover, if phage resistance could be prevented entirely, effective phage therapy  
307 would require a lower lung neutrophil counts of at least 20% and 10% of healthy patients as  
308 predicted by the *PS-R* (Fig. S4E) and *HM-R* (Fig. S4F) models, respectively.

309

### 310 **Phage prophylaxis of acute respiratory infection**

311 Antimicrobial prophylaxis is commonly used for the prevention of numerous infectious diseases,  
312 including *P. aeruginosa* respiratory infection (Stanojevic et al., 2014). We first determined that  
313 phage PAK\_P1 was gradually eliminated from the lungs of mice with an exponential decay

314 constant of approximately 0.5 log/d after a single intranasal dose of  $10^9$  PFU (Table S2).  
315 Leveraging this result, we find that inhaled phages could provide prophylaxis by preventing  
316 pneumonia in 100% of challenged wild-type immunocompetent mice if given up to 4d prior to  
317 bacterial challenge (Fig. 6A). Prophylaxis could also be achieved in *Rag2<sup>-/-</sup>Il2rg<sup>-/-</sup>* mice (Fig. S5).  
318 We estimate that initial phage densities would be about  $10^6$  PFU at the time of infectious  
319 challenge given prophylactic dose and decay rates (Table S2). This prophylactic dose yields an  
320 effective treatment MOI of 0.1, which is 100-fold lower than our curative treatment dose (Fig.  
321 1). Nonetheless, the relative changes within *in vivo* bioluminescence dissemination, proliferation,  
322 and resolution profiles were similar between phage prophylaxis and ‘curative’ phage therapy  
323 (compare Figs. 6B and 1C, respectfully). We utilized both *HM-R* (Fig. 6C) and *PS-R* (Fig. 6D)  
324 models to evaluate the prophylactic potential of phages, using the same parameters as with  
325 ‘curative’ phage therapy except adjusting the point of phage administration to -4d and using a  
326 prophylactic dose equivalent to  $10^9$  PFU (Table S1). Both mathematical models similarly predict  
327 effective phage prophylaxis in immunocompetent hosts. We demonstrate that the lower phage  
328 dose at the time of infectious challenge does not exert a strong effect on efficacy, likely due to  
329 the rapid replication of resident phages when bacteria are introduced. It remains unclear as to  
330 whether prophylactic application also provides greater time for penetration into the lung,  
331 potentially reducing the slowdown of phage lysis due to spatial heterogeneity.

332

### 333 **Absence of evidence for direct activation of the immune system by phage PAK\_P1**

334 Previous studies have yet to adequately address if phages themselves promote recruitment of  
335 immune effector cells to the site of infection, or if phage prophylaxis primes immune cells to a  
336 state of enhanced defense (El-Benna et al., 2016). As cytokines control the dynamics of immune

337 cell behavior and initiate inflammation (Eberl et al., 2015), we sought to examine whether phage  
338 PAK\_P1 at the high dose of  $10^9$  PFU could stimulate the production of a panel of cytokines in  
339 immunocompetent mouse lung tissues. We found that a high phage dose did not significantly  
340 increase the production of cytokines compared to the PBS control over 4d (Figs. 6E and S6).  
341 More importantly, phage-exposed lungs harbored significantly lower cytokine levels than lungs  
342 assaulted with lipopolysaccharide (LPS). Our data coincides with other studies (Bocian et al.,  
343 2016). This suggests that phage PAK\_P1 was immunologically well tolerated, and it was  
344 unlikely that phage presence promoted further recruitment or primed immune cells during  
345 treatment. Accordingly, we did not include direct activation of host immunity by phages in our  
346 mathematical population models. Importantly, phage immunotolerance may be phage type and  
347 setting dependent.

348

349 A further concern regarding phage therapy is that the host immunity will neutralize the  
350 administered phages (Lusiak-Szelachowska et al., 2016). It has been suggested that innate  
351 immunity may be sufficient for rapid clearance of phages from circulation (Merril et al., 1996).  
352 However, we find no evidence of this, as phage PAK\_P1 demonstrated a high degree of  
353 persistence in the airways of all tested uninfected mice (Table S2). However, immunodeficiency  
354 did prolong persistence of phage in the mouse lungs by day 4 ( $p < 0.001$ ). Some caution is  
355 warranted given that mice received only a single phage treatment dose. Repeated phage doses  
356 might promote a stronger antigen-specific neutralizing response, but previous studies are  
357 equivocal as to whether this would occur (Bruttin and Brussow, 2005; Lusiak-Szelachowska et  
358 al., 2014; Majewska et al., 2015). For example, weeks of oral application of phages did result in  
359 anti-phage neutralizing antibodies in mice (Majewska et al., 2015), but long-term oral

360 application in humans did not (Bruttin and Brussow, 2005). Nonetheless, if and how the host  
361 immune system senses and responds to phage warrants further investigation.

362

### 363 **Discussion**

364 In this study, we show that successful phage curative and prophylactic therapies of acute  
365 respiratory infections depends on an essential synergy between phage lysis and the host's own  
366 immune defenses, a concept we term "immunophage synergy". In comparing phage treatment  
367 efficacies in murine hosts with distinct types of immunodeficiency, namely MyD88 deficient,  
368 lymphocyte deficient, and severe neutropenia, we have identified that phage-neutrophil synergy  
369 leads to resolution of acute infection. Utilizing *in silico* population modeling of phage therapy  
370 given systematic modulation of host innate immune responses, we provided further support for a  
371 mechanism by which host neutrophils are required to control both phage-sensitive and emergent  
372 phage-resistant variants to ensure infection eradication. Our *in vivo* results also demonstrate the  
373 efficacy of phage prophylaxis. *In silico* population modeling implies that both the slow  
374 elimination of phage from the lungs and the self-amplification of phage contribute to the  
375 prophylactic success. Further, we find that phages are immunologically well tolerated and were  
376 not significantly neutralized in the lungs by immune defenses. Our data supports a distinct  
377 interpretation of phage therapy than the prevailing paradigms. From a translational perspective,  
378 the current findings also suggest the need to revisit appropriate patient immunological inclusion  
379 criterion before phage therapies are employed.

380

381 Resistance development is a major hurdle with all antimicrobial therapies. Here, we modeled  
382 monophage therapy with a single virus type, namely phage PAK\_P1. Our results provide a  
383 mechanistic basis to explain experimental observations that phage resistance can emerge but

384 does not result in therapeutic failure in healthy immunocompetent hosts (Bull et al., 2002; Smith  
385 and Huggins, 1982). Rather, treatment failure is caused when host innate immune defenses fail to  
386 eliminate phage-resistant subpopulations. We therefore speculate that resistance would not  
387 render phage therapy ineffective as long as a substantial ratio of the targeted bacterial population  
388 is sensitive to phage infection. While our study is limited in scope to monophage therapy,  
389 polyphage therapy (i.e. a mixture of different phage types) is often used to reduce the risk of  
390 emergent phage resistance (Pabary et al., 2016). However, our *in silico* analysis also predicts that  
391 even if the bacterial population was entirely phage-sensitive (i.e. no resistant mutants), phages  
392 alone would still be unlikely to eradicate the bacterial burden in the lungs (Levin et al., 1977;  
393 Weitz, 2015). This suggests polyphage therapy will also need immunophage synergy to resolve  
394 acute infections. Our study also does not evaluate the feasibility and effect of combining phage  
395 with other antibacterials, such as small molecule antibiotics (Chan et al., 2016). The effects of  
396 host immunity on antibiotic efficacy will also need to be considered alongside immunophage  
397 synergy. In addition, combination therapies may be able to augment host immune responses in  
398 settings of weakened immunity to combat both phage-sensitive and phage-resistant populations.  
399

400 Immunophage synergy is of relevance to ongoing efforts to understand the basic mechanisms  
401 and clinical potential of phage therapy. Our results suggest that ILCs are not key players in the  
402 immunophage synergy to resolve acute infection. At the mucosa of the lungs mouse ILCs are  
403 thought to respond to pathogens indirectly by sensing myeloid-cell- or epithelial-cell-derived  
404 cytokines and to further promoting immune defenses by further secreting immune effector  
405 mediators (Eberl et al., 2015). ILC absence might also cause a reduction in overall innate  
406 immune activation and recruitment similar to Myd88 deficiency, but at a less drastic level.

407 Modest immune response reductions due to ILC loss need not lead to therapeutic failure, given  
408 that our population models predict that 20-50% of a healthy innate immune response would be  
409 sufficient for successful phage therapy (Fig. 3E and S4). In generalizing the current framework  
410 for humans, a limitation of our study is that mouse ILCs lack PRRs (Eberl et al., 2015). In  
411 contrast, human ILC3s can express PRRs, like TLRs, which could receive additional signaling  
412 directly through bacterial stimulation. Together, we cannot rule out that ILCs have an additive  
413 contribution to immunophage synergy. Furthermore, adaptive humoral responses (B cells) and  
414 cellular responses (T cells) are expected to play a greater role in immunophage synergy in  
415 resolving chronic infections.

416

417 We have not determined whether the observed failure of phage therapy due to innate immunity  
418 deficiencies was due to a loss of neutrophil effector functions (e.g., phagocytosis and NETosis)  
419 or the absence of neutrophil-dependent activation of other immune effector components that also  
420 promote clearance of *P. aeruginosa*. As both likely play a role, future experiments studying mild  
421 neutropenia and neutrophil dysfunction could elucidate the innate immune mechanisms involved  
422 in efficient phage therapy. This may in turn lead to alteration of phage therapy formulations, or  
423 even novel phage-antibiotic combinations, to enhance treatments in hosts with weakened  
424 immunity. Besides likely extending beyond acute respiratory infections to other infectious  
425 diseases, the status of the innate immune response, including concentrations and activity of  
426 neutrophils and other effector cells, depend on disease status, environment, and genetic factors  
427 (Heron et al., 2012).

428

429 There are multiple ways that the current immunophage synergy framework could be extended.

430 First, the current experimental and modeling framework could be used to test the efficacy of  
431 polyphage therapies, given trade-offs between coverage of types and relative densities in the  
432 initial therapeutic phage doses. The adaptation of the *in silico* population model to the *in vivo*  
433 context included the hypothesis that killing rate of bacteria by phage increases sublinearly with  
434 phage densities. Our prior analysis of the PoP phage therapeutic model showed that explicit  
435 modeling of the infected cell state did not change qualitative outcomes of therapy (Leung and  
436 Weitz, 2016). Future analysis of the current therapeutic model may also consider how  
437 predictions are affected by fixed delays between infection and lysis (Levin et al., 1977) and/or  
438 changes in cell state at high densities that suppress phage replication (Levin et al., 1977; Weitz  
439 and Dushoff, 2008). Moving forward, it will be worthwhile to develop population models and  
440 experimental methods to test the “microscale” mode of action, e.g., by resolving the joint, spatial  
441 dynamics of bacteria, phage, and neutrophils during treatment. In doing so, we anticipate that  
442 incorporation of stochastic, individual-based models may shed light on how microscale  
443 heterogeneity influences the quantitative time-course of dynamics of therapeutic intervention at  
444 population scales. Efforts to resolve spatially-explicit phage-bacteria interactions have already  
445 shed light on how viruses disrupt micro-colonies or biofilms *in vitro* and could be productively  
446 adapted for *in vivo* studies (Azeredo and Sutherland, 2008).

447

448 To conclude, association of *in vivo* and *in silico* modeling of human infectious disease provided a  
449 framework in studying outcomes arising from the tripartite interactions between phage, bacteria  
450 and host immunity. Although, this framework was built here to support the development of  
451 phage therapies, it will also be of value in a more general context to comprehensively decipher  
452 phage, bacteria and host immune cell population dynamics in human microbiomes (Debarbieux,

453 2014; Mirzaei and Maurice, 2017).

454

455 **Author contributions**

456 DRR, JDS, JSW and LD conceived the experiments. DRR, EM and MH performed experiments.  
457 CYL and DS performed mathematical modeling. CYL, DRR, JDS, JSW and LD analyzed the  
458 data. CYL, DRR, JSW and LD wrote the manuscript.

459

460 **Acknowledgements:**

461 We thank N. Dufour, C. Archambeau, and E. Atse (Microbiology, Institut Pasteur), H. Strick-  
462 Marchand (Immunology, Institut Pasteur), M.A Nicola (Imagopole, Institut Pasteur) and Center  
463 for Human Immunology at Institut Pasteur for their technical support. We thank S. Chollet-  
464 Martin (U Paris-Sud) for her comments about the manuscript. We thank J. Bull (UT-Austin) and  
465 another reviewer for their feedback. This study was supported by the Fondation EDF, the  
466 Association Vaincre la Mucoviscidose [IC1011], the Association CA. ZO. LA. Luttons contre la  
467 mucoviscidose, and the U.S. Army Research Office [W911NF-14-1-0402]. DRR is the recipient  
468 of a European Respiratory Society Fellowship [RESPIRE2–2015–8416].

469

470

471 **References**

- 472 Abedon, S.T. (2009). Kinetics of phage-mediated biocontrol of bacteria. *Foodborne Pathog Dis*  
473 *6*, 807-815.
- 474 Abedon, S.T., Kuhl, S.J., Blasdel, B.G., and Kutter, E.M. (2011). Phage treatment of human  
475 infections. *Bacteriophage 1*, 66-85.
- 476 Adams, M.H. (1959). *Bacteriophages* (Interscience Publishers).
- 477 Albanesi, M., Mancardi, D.A., Jonsson, F., Iannascoli, B., Fiette, L., Di Santo, J.P., Lowell,  
478 C.A., and Bruhns, P. (2013). Neutrophils mediate antibody-induced antitumor effects in mice.  
479 *Blood 122*, 3160-3164.
- 480 Andreu, N., Zelmer, A., and Wiles, S. (2011). Noninvasive biophotonic imaging for studies of  
481 infectious disease. *FEMS Microbiol Rev 35*, 360-394.
- 482 Azeredo, J., and Sutherland, I.W. (2008). The use of phages for the removal of infectious  
483 biofilms. *Curr Pharm Biotechnol 9*, 261-266.
- 484 Bansal, S., Grenfell, B.T., and Meyers, L.A. (2007). When individual behaviour matters:  
485 homogeneous and network models in epidemiology. *J R Soc Interface 4*, 879-891.
- 486 Barletta, K.E., Cagnina, R.E., Wallace, K.L., Ramos, S.I., Mehrad, B., and Linden, J. (2012).  
487 Leukocyte compartments in the mouse lung: distinguishing between marginated, interstitial, and  
488 alveolar cells in response to injury. *J Immunol Method 375*, 100-110.
- 489 Bocian, K., Borysowski, J., Zarzycki, M., Pacek, M., Weber-Dabrowska, B., Machcinska, M.,  
490 Korczak-Kowalska, G., and Gorski, A. (2016). The Effects of T4 and A3/R Bacteriophages on  
491 Differentiation of Human Myeloid Dendritic Cells. *Frontiers in microbiology 7*, 1267.
- 492 Bohannan, B.J., Kerr, B., Jessup, C.M., Hughes, J.B., and Sandvik, G. (2002). Trade-offs and  
493 coexistence in microbial microcosms. *Antonie van Leeuwenhoek 81*, 107-115.

494 Brogan, D.M., and Mossialos, E. (2016). A critical analysis of the review on antimicrobial  
495 resistance report and the infectious disease financing facility. *Global Health* 12, 8.

496 Brown, C.M., and Bidle, K.D. (2014). Attenuation of virus production at high multiplicities of  
497 infection in *Aureococcus anophagefferens*. *Virology* 466-467, 71-81.

498 Bruttin, A., and Brussow, H. (2005). Human volunteers receiving *Escherichia coli* phage T4  
499 orally: a safety test of phage therapy. *Antimicrob Agents Chemother* 49, 2874-2878.

500 Bull, J.J., Levin, B.R., DeRouin, T., Walker, N., and Bloch, C.A. (2002). Dynamics of success  
501 and failure in phage and antibiotic therapy in experimental infections. *BMC Microbiol* 2, 35.

502 Campbell, A. (1961). Conditions for the Existence of Bacteriophage. *Evolution* 15, 153-165.

503 CDC (2013). Antibiotic resistance threats in the United States (Available at:  
504 <http://www.cdc.gov/drugresistance/threat-report-2013>: US Centers for Disease Control and  
505 Prevention).

506 Chan, B.K., Siström, M., Wertz, J.E., Kortright, K.E., Narayan, D., and Turner, P.E. (2016).  
507 Phage selection restores antibiotic sensitivity in MDR *Pseudomonas aeruginosa*. *Sci Rep* 6,  
508 26717.

509 Colucci, F., Soudais, C., Rosmaraki, E., Vanes, L., Tybulewicz, V.L., and Di Santo, J.P. (1999).  
510 Dissecting NK cell development using a novel alymphoid mouse model: investigating the role of  
511 the c-abl proto-oncogene in murine NK cell differentiation. *J Immunol* 162, 2761-2765.

512 Czaplewski, L., Bax, R., Clokie, M., Dawson, M., Fairhead, H., Fischetti, V.A., Foster, S.,  
513 Gilmore, B.F., Hancock, R.E., Harper, D., *et al.* (2016). Alternatives to antibiotics-a pipeline  
514 portfolio review. *Lancet Infect Dis* 16, 239-251.

515 Debarbieux, L. (2014). Bacterial sensing of bacteriophages in communities: the search for the  
516 Rosetta stone. *Curr Opin Microbiol* 20, 125-130.

517 Debarbieux, L., Leduc, D., Maura, D., Morello, E., Criscuolo, A., Grossi, O., Balloy, V., and  
518 Touqui, L. (2010). Bacteriophages can treat and prevent *Pseudomonas aeruginosa* lung  
519 infections. *J Infect Dis* 201, 1096-1104.

520 Dennehy, J.J. (2012). What Can Phages Tell Us about Host-Pathogen Coevolution? *Int J Evol*  
521 *Biol* 2012, 396165.

522 Drusano, G.L., Vanscoy, B., Liu, W., Fikes, S., Brown, D., and Louie, A. (2011). Saturability of  
523 granulocyte kill of *Pseudomonas aeruginosa* in a murine model of pneumonia. *Antimicrob*  
524 *Agents Chemother* 55, 2693-2695.

525 Eberl, G., Colonna, M., Di Santo, J.P., and McKenzie, A.N. (2015). Innate lymphoid cells.  
526 Innate lymphoid cells: a new paradigm in immunology. *Science* 348.

527 El-Benna, J., Hurtado-Nedelec, M., Marzaioli, V., Marie, J.C., Gougerot-Pocidallo, M.A., and  
528 Dang, P.M. (2016). Priming of the neutrophil respiratory burst: role in host defense and  
529 inflammation. *Immunological reviews* 273, 180-193.

530 Florens, M., Sapoval, B., and Filoche, M. (2011). An anatomical and functional model of the  
531 human tracheobronchial tree. *J Appl Physiol* 110, 756-763.

532 Henry, M., Bobay, L.M., Chevallereau, A., Saussereau, E., Ceysens, P.J., and Debarbieux, L.  
533 (2015). The search for therapeutic bacteriophages uncovers one new subfamily and two new  
534 genera of *Pseudomonas*-infecting *Myoviridae*. *PLoS One* 10, e0117163.

535 Henry, M., Lavigne, R., and Debarbieux, L. (2013). Predicting *in vivo* efficacy of therapeutic  
536 bacteriophages used to treat pulmonary infections. *Antimicrob Agents Chemother* 57, 5961-  
537 5968.

538 Heron, M., Grutters, J.C., ten Dam-Molenkamp, K.M., Hijdra, D., van Heugten-Roeling, A.,  
539 Claessen, A.M., Ruven, H.J., van den Bosch, J.M., and van Velzen-Blad, H. (2012).  
540 Bronchoalveolar lavage cell pattern from healthy human lung. *Clin Exp Immunol* 167, 523-531.  
541 Kawai, T., Adachi, O., Ogawa, T., Takeda, K., and Akira, S. (1999). Unresponsiveness of  
542 MyD88-deficient mice to endotoxin. *Immunity* 11, 115-122.  
543 Knoll, B.M., and Mylonakis, E. (2014). Antibacterial bioagents based on principles of  
544 bacteriophage biology: an overview. *Clin Infect Dis* 58, 528-534.  
545 Kolaczkowska, E., and Kubes, P. (2013). Neutrophil recruitment and function in health and  
546 inflammation. *Nat Rev Immunol* 13, 159-175.  
547 Leung, C.Y., and Weitz, J.S. (2016). Synergistic elimination of bacteria by phage and the  
548 immune system. *bioRxiv* 057927.  
549 Levin, B.R., and Bull, J.J. (1996). Phage Therapy Revisited: The Population Biology of a  
550 Bacterial Infection and Its Treatment with Bacteriophage and Antibiotics. *The American*  
551 *Naturalist* 147, 881-898.  
552 Levin, B.R., and Bull, J.J. (2004). Population and evolutionary dynamics of phage therapy. *Nat*  
553 *Rev Microbiol* 2, 166-173.  
554 Levin, B.R., Stewart, F.M., and Chao, L. (1977). Resource-Limited Growth, Competition, and  
555 Predation: A Model and Experimental Studies with Bacteria and Bacteriophage. *The American*  
556 *Naturalist* 111, 3-24.  
557 Li, Y., Karlin, A., Loike, J.D., and Silverstein, S.C. (2002). A critical concentration of  
558 neutrophils is required for effective bacterial killing in suspension. *Proc Natl Acad Sci U S A* 99,  
559 8289-8294.

560 Liu, W.M., Hethcote, H.W., and Levin, S.A. (1987). Dynamical behavior of epidemiological  
561 models with nonlinear incidence rates. *J Math Biol* 25, 359-380.

562 Luria, S.E., and Delbruck, M. (1943). Mutations of bacteria from virus sensitivity to virus  
563 resistance. *Genetics* 28, 491-511.

564 Lusiak-Szelachowska, M., Zaczek, M., Weber-Dabrowska, B., Miedzybrodzki, R., Klak, M.,  
565 Fortuna, W., Letkiewicz, S., Rogoz, P., Szufnarowski, K., Jonczyk-Matysiak, E., *et al.* (2014).  
566 Phage neutralization by sera of patients receiving phage therapy. *Viral Immunol* 27, 295-304.

567 Lusiak-Szelachowska, M., Zaczek, M., Weber-Dabrowska, B., Miedzybrodzki, R., Letkiewicz,  
568 S., Fortuna, W., Rogoz, P., Szufnarowski, K., Jonczyk-Matysiak, E., Olchawa, E., *et al.* (2016).  
569 Antiphage activity of sera during phage therapy in relation to its outcome. *Future microbiology*.  
570 Majewska, J., Beta, W., Lecion, D., Hodyra-Stefaniak, K., Klopot, A., Kazmierczak, Z.,  
571 Miernikiewicz, P., Piotrowicz, A., Ciekot, J., Owczarek, B., *et al.* (2015). Oral application of T4  
572 phage induces weak antibody production in the gut and in the blood. *Viruses* 7, 4783-4799.

573 Mazurier, F., Fontanellas, A., Salesse, S., Taine, L., Landriau, S., Moreau-Gaudry, F., Reiffers,  
574 J., Peault, B., Di Santo, J.P., and de Verneuil, H. (1999). A novel immunodeficient mouse  
575 model--RAG2 x common cytokine receptor gamma chain double mutants--requiring exogenous  
576 cytokine administration for human hematopoietic stem cell engraftment. *J Interferon Cytokine*  
577 *Res* 19, 533-541.

578 Merrill, C.R., Biswas, B., Carlton, R., Jensen, N.C., Creed, G.J., Zullo, S., and Adhya, S. (1996).  
579 Long-circulating bacteriophage as antibacterial agents. *Proc Natl Acad Sci U S A* 93, 3188-3192.

580 Meyer, J.R., Dobias, D.T., Weitz, J.S., Barrick, J.E., Quick, R.T., and Lenski, R.E. (2012).  
581 Repeatability and contingency in the evolution of a key innovation in phage lambda. *Science*  
582 335, 428-432.

583 Mirzaei, M.K., and Maurice, C.F. (2017). Menage a trois in the human gut: interactions between  
584 host, bacteria and phages. *Nat Rev Microbiol*.

585 Moir, D.T., Ming, D., Opperman, T., Schweizer, H.P., and Bowlin, T.L. (2007). A high-  
586 throughput, homogeneous, bioluminescent assay for *Pseudomonas aeruginosa* gyrase inhibitors  
587 and other DNA-damaging agents. *J Biomol Screen* 12, 855-864.

588 Munder, A., Wolbeling, F., Klockgether, J., Wiehlmann, L., and Tummeler, B. (2014). In vivo  
589 imaging of bioluminescent *Pseudomonas aeruginosa* in an acute murine airway infection model.  
590 *Pathog Dis* 72, 74-77.

591 Murray, J.L., Kwon, T., Marcotte, E.M., and Whiteley, M. (2015). Intrinsic Antimicrobial  
592 Resistance Determinants in the Superbug *Pseudomonas aeruginosa*. *mBio* 6, e01603-01615.

593 Newburger, P.E., and Dale, D.C. (2013). Evaluation and management of patients with isolated  
594 neutropenia. *Semin Hematol* 50, 198-206.

595 Pabary, R., Singh, C., Morales, S., Bush, A., Alshafi, K., Bilton, D., Alton, E.W., Smithyman,  
596 A., and Davies, J.C. (2016). Antipseudomonal bacteriophage reduces infective burden and  
597 inflammatory response in murine lung. *Antimicrob Agents Chemother* 60, 744-751.

598 Reutershan, J., Basit, A., Galkina, E.V., and Ley, K. (2005). Sequential recruitment of  
599 neutrophils into lung and bronchoalveolar lavage fluid in LPS-induced acute lung injury. *Am J*  
600 *Physiol Lung Cell Mol Physiol* 289, L807-815.

601 Rhoads, D.D., Wolcott, R.D., Kuskowski, M.A., Wolcott, B.M., Ward, L.S., and Sulakvelidze,  
602 A. (2009). Bacteriophage therapy of venous leg ulcers in humans: results of a phase I safety trial.  
603 *J Wound Care* 18, 237-238, 240-233.

604 Roach, D.R., and Debarbieux, L. (2017). Phage therapy: awakening a sleeping giant. *Emerging*  
605 *Topics in Life Sciences* 1, 93-103.

606 Roy, M., and Pascual, M. (2006). On representing network heterogeneities in the incidence rate  
607 of simple epidemic models. *Ecol Complex* 3, 80-90.

608 Salmond, G.P., and Fineran, P.C. (2015). A century of the phage: past, present and future. *Nat*  
609 *Rev Microbiol* 13, 777-786.

610 Salsgiver, E.L., Fink, A.K., Knapp, E.A., LiPuma, J.J., Olivier, K.N., Marshall, B.C., and  
611 Saiman, L. (2016). Changing Epidemiology of the Respiratory Bacteriology of Patients With  
612 Cystic Fibrosis. *Chest* 149, 390-400.

613 Sarker, S.A., Berger, B., Deng, Y., Kieser, S., Foata, F., Moine, D., Descombes, P., Sultana, S.,  
614 Huq, S., Bardhan, P.K., *et al.* (2016a). Oral application of Escherichia coli bacteriophage: safety  
615 tests in healthy and diarrheal children from Bangladesh. *Environ Microbiol.*

616 Sarker, S.A., Sultana, S., Reuteler, G., Moine, D., Descombes, P., Charton, F., Bourdin, G.,  
617 McCallin, S., Ngom-Bru, C., Neville, T., *et al.* (2016b). Oral Phage Therapy of Acute Bacterial  
618 Diarrhea With Two Coliphage Preparations: A Randomized Trial in Children From Bangladesh.  
619 *EBioMedicine* 4, 124-137.

620 Skerrett, S.J., Liggitt, H.D., Hajjar, A.M., and Wilson, C.B. (2004). Cutting edge: myeloid  
621 differentiation factor 88 is essential for pulmonary host defense against *Pseudomonas*  
622 *aeruginosa* but not *Staphylococcus aureus*. *J Immunol* 172, 3377-3381.

623 Smith, H.W., and Huggins, M.B. (1982). Successful treatment of experimental Escherichia coli  
624 infections in mice using phage: its general superiority over antibiotics. *J Gen Microbiol* 128,  
625 307-318.

626 Stanojevic, S., Waters, V., Mathew, J.L., Taylor, L., and Ratjen, F. (2014). Effectiveness of  
627 inhaled tobramycin in eradicating *Pseudomonas aeruginosa* in children with cystic fibrosis. *J*  
628 *Cyst Fibros* 13, 172-178.

629 Vandenhoevel, D., Lavigne, R., and Brussow, H. (2015). Bacteriophage Therapy: Advances in  
630 Formulation Strategies and Human Clinical Trials. *Annu Rev Virol* 2, 599-618.

631 Warner, N., and Nunez, G. (2013). MyD88: a critical adaptor protein in innate immunity signal  
632 transduction. *J Immunol* 190, 3-4.

633 Weibel, E.R. (1963). *Morphometry of the human lung* (Academic Press).

634 Weitz, J.S. (2015). *Quantitative viral ecology: Dynamics of viruses and their microbial hosts*  
635 (Princeton, New Jersey: Princeton University Press).

636 Weitz, J.S., and Dushoff, J. (2008). Alternative stable states in host–phage dynamics. *Theoretical*  
637 *Ecology* 1, 13-19.

638 Zhang, Z., Louboutin, J.P., Weiner, D.J., Goldberg, J.B., and Wilson, J.M. (2005). Human  
639 airway epithelial cells sense *Pseudomonas aeruginosa* infection via recognition of flagellin by  
640 Toll-like receptor 5. *Infect Immun* 73, 7151-7160.

641

642

643

## Figures legends

644  
645  
646  
647  
648  
649  
650  
651  
652  
653  
654  
655  
656

**Fig. 1. Immunophage therapy efficacy in the immunocompetent host.** (A) Post treatment representative *in vivo* imaging of bioluminescent *Pseudomonas aeruginosa* infected live mice; color scale is radiance ( $\text{p/s}^2/\text{cm}^2/\text{sr}$ ). (B) Single dose inhaled monophage treatment (MOI of 10) of fatal acute respiratory infection by *P. aeruginosa* ( $10^7$  CFU) after a 2h delay provided immunocompetent wild-type mice 100% survival probability compared to saline-mock treated control group (n=6 per group). (C) Colonization pattern of the bioluminescent *P. aeruginosa* in the lungs of live mice plotted as mean radiance over time indicating phage antibacterial activity by a significant reduction in bacterial burden beyond 2h post treatment. Arrow marks treatment point; *in vivo* radiance limit of detection (LOD); error bars indicate SEM. [\*  $p < 0.05$ ; \*\*\*  $p < 0.001$ ]

657 **Fig. 2. Phage therapy eliminates bacteria in mathematical models of phage therapy in**  
658 **immunocompetent host.** (A) Schematic diagram of models with host immunity (I), bacteria (B)  
659 and phages (P) interactions accounting for heterogeneous mixing (HM) or phage saturation (PS),  
660 which differ only in the phage lysis rate. Phages are assumed to be cleared at a constant rate.  
661 Simulated bacteria, phage and immune densities with (B) HM or (C) PS parameters. (D)  
662 Schematic diagram of heterogeneous mixing-resistance (HM-R) or phage saturation-resistance  
663 (PS-R) models with the addition of phage-resistant mutants as a subpopulation of target bacteria.  
664 The dotted compartment denotes the total bacterial population, which is the sum of the sensitive  
665 (S) and resistant (R) subpopulations. Predicted population densities with (E) HM-R or (F) PS-R  
666 models. All simulations predict phage-sensitive and phage-resistant bacterial elimination during

667 phage therapy in hosts with a fully functioning innate immune response. See Table S1 for *in*  
668 *silico* simulation parameters.

669

670 **Fig. 3. Phage therapy is inefficient in the innate immunity activation deficient host. (A)**

671 Myeloid differentiation primary response gene 88 deficient mice (*MyD88*<sup>-/-</sup>) had a 15% survival  
672 probability of acute respiratory infection by *Pseudomonas aeruginosa* (10<sup>5</sup> CFU) when inhaled  
673 monophage therapy (MOI of 10) was given at 2h post infection compared to saline-mock treated  
674 (n=15 per group). In contrast, wild-type mice recovered from the 10<sup>5</sup> CFU challenge without

675 phage treatment **(B)** Colonization pattern of the bioluminescent pathogen in the mouse lungs  
676 plotted as mean radiance (p/s<sup>2</sup>/cm<sup>2</sup>/sr) over time to indicate phage antibacterial activity by a brief  
677 reduction in bacterial load followed by outgrowth of phage-resistant clone post infection. Arrow  
678 marks treatment point; *in vivo* radiance limit of detection (LOD); error bars indicate SEM. [\* p<

679 0.05; \*\*\* p< 0.001] **(C)** Heterogeneous mixing (*HM-R*) and **(D)** phage saturation (*PS-R*) model  
680 simulations of hosts lacking innate immunity activation and the effect on phage-sensitive and  
681 phage-resistant bacterial densities during phage treatment. Both models predict that phage-  
682 resistant bacteria outgrowth replaces the sensitive population. **(E)** *HM-R* model prediction of the

683 level of innate immune activation relative to immunocompetent hosts needed to eliminate phage-  
684 resistant bacterial outgrowth and restore phage therapy efficacy in this setting. The curves show  
685 the sum of sensitive and resistant bacterial densities. See Table S1 for *in silico* simulation  
686 parameters.

687

688 **Fig. 4. Phage therapy is efficient in the innate and adaptive lymphocyte deficient host. (A)**

689 Inhaled monophage therapy (MOI of 10) after a 2h delay provided lymphocyte deficient *Rag2*<sup>-/-</sup>

690 *Il2rg*<sup>-/-</sup> mice a 90% survival probability from acute respiratory infection by *Pseudomonas*  
691 *aeruginosa* (10<sup>7</sup> CFU; n=6 per group). **(B)** Bioluminescent pathogen mean radiance (p/s<sup>2</sup>/cm<sup>2</sup>/sr)  
692 in the lungs of live mice over time to indicate bacterial colonization pattern and phage  
693 bacteriolytic activity by a significant reduction in bacterial burden beyond 2h post treatment.  
694 Arrow marks treatment point; *in vivo* radiance limit of detection (LOD); error bars indicate SEM.  
695 [\* p< 0.05; \*\*\* p< 0.001]

696

697

698 **Fig. 5. Phage therapy is ineffective in the neutropenic host.** Anti-granulocyte receptor-1 (Gr1)  
699 monoclonal antibody was used to deplete neutrophils in wild-type mice 24h before an intranasal  
700 inoculum of *Pseudomonas aeruginosa* (10<sup>5</sup> CFU; n=4 per group). After a 2h delay, these  
701 neutropenic mice received a single dose inhaled monophage therapy (MOI of 10), which was  
702 ineffective in preventing fatal pneumonia. **(B)** Colonization pattern of the bioluminescent  
703 pathogen in the lungs of live mice plotted as mean radiance (p/s<sup>2</sup>/cm<sup>2</sup>/sr) over time showed no  
704 indication of phage antibacterial activity. Arrow marks treatment point; *in vivo* radiance limit of  
705 detection (LOD); error bars indicate SEM. **(C-E)** *In silico* simulations of phage therapy in  
706 neutrophil-depleted hosts modeled by setting host innate immune response to zero. Time series  
707 of bacteria, phage and immune cell populations from **(C)** heterogeneous mixing (*HM-R*) and **(D)**  
708 phage saturation (*PS-R*) models both predicting a decline of sensitive bacteria over time  
709 accompanied by dominance of phage-resistant outgrowth causing phage therapy failure. **(E)**  
710 *HM-R* model prediction of the level of neutrophil activity relative to healthy hosts required to  
711 eliminate phage-resistant bacterial outgrowth and restore phage therapy efficacy in neutropenic  
712 hosts. The curves show the total bacterial population densities. See Table S1 for *in silico*

713 simulation parameters.

714

715 **Fig. 6. Efficient non-immune priming phage prophylaxis in the immunocompetent host. (A)**

716 Wild-type mice received a single inhaled monophage dose ( $10^9$  PFU) which gave prophylaxis for

717 4d against *P. aeruginosa* ( $10^7$  CFU; n=6 per group). **(B)** Luminescence plotted as mean radiance

718 ( $\text{p/s}^2/\text{cm}^2/\text{sr}$ ) from bacteria over time demonstrates phages maintain antibacterial activity after

719 residing in the mouse lungs for 4d. Arrow indicates treatment point; *in vivo* radiance limit of

720 detection (LOD); error bars indicate SEM. [\*\*  $p < 0.01$ ; \*\*\*  $p < 0.001$ ] **(C)** Heterogeneous

721 mixing (*HM-R*) and **(D)** phage saturation (*PS-R*) model simulations of phage prophylaxis in

722 immunocompetent hosts both predict that a slow decay of phage density would occur before the

723 phage outgrowth following bacterial inoculation, which leads to bacterial burden elimination.

724 See Table S1 for *in silico* simulation parameters. **(E)** Differential production of cytokines in

725 mouse lung tissues after exposure to 10  $\mu\text{g}$  *P. aeruginosa* LPS, PBS, or phages ( $10^9$  PFU)

726 suggests that significant priming of host immunity by phage PAK\_P1 does not occur. However,

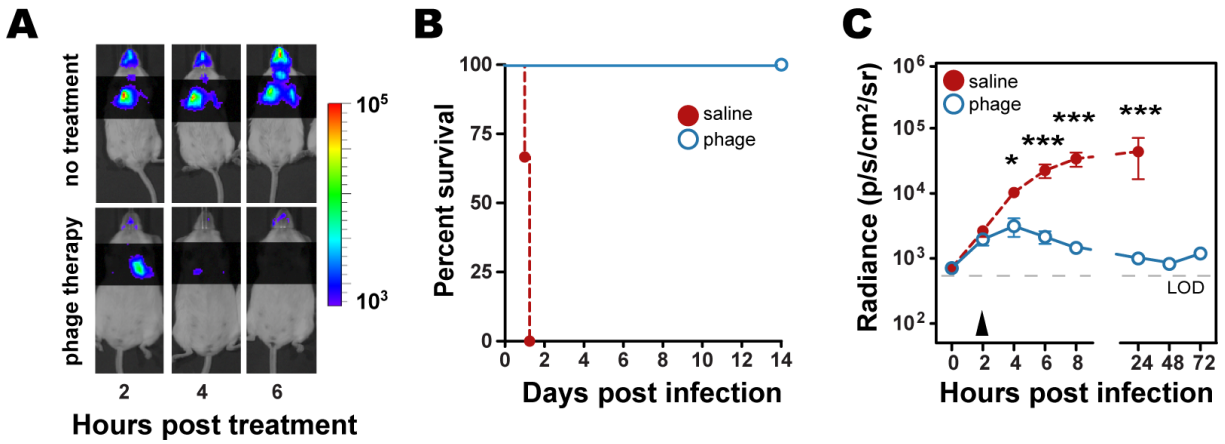
727  $\text{IFN}\gamma$  and  $\text{TNF}\alpha$  production was significantly lower in phage exposed compared to PBS exposed

728 lungs [Welches t-test;  $p < 0.05$ ]. For values see Fig. S6.

729

730

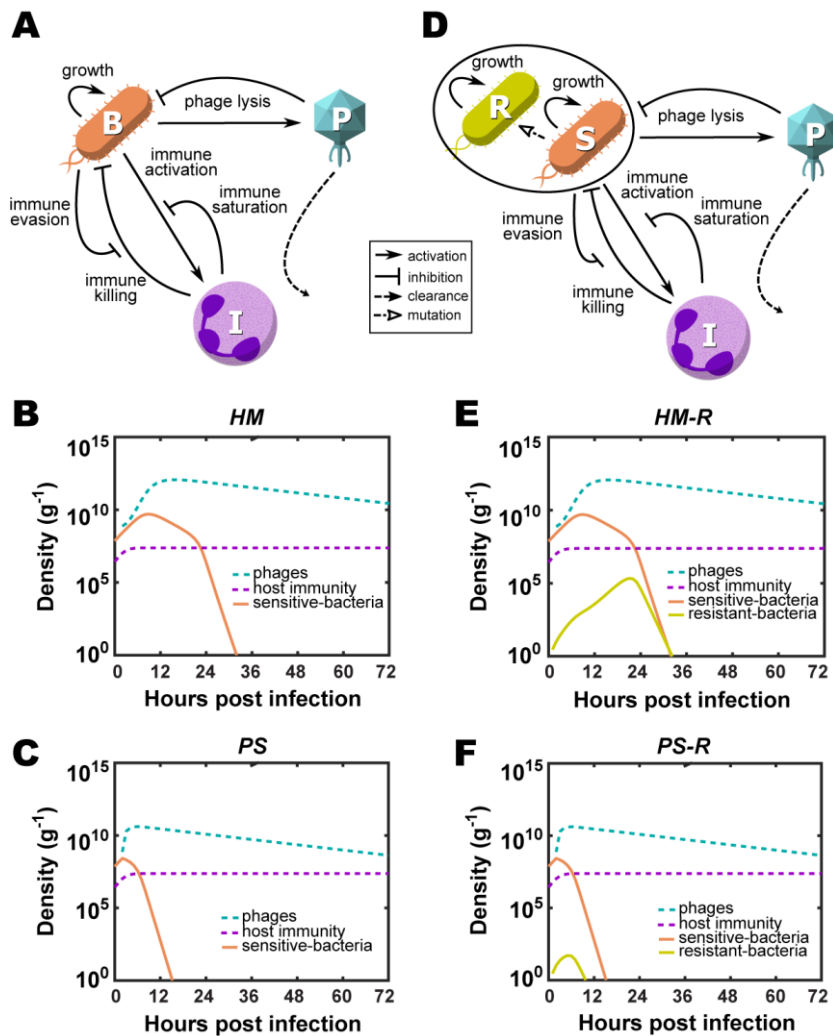
731 Figure 1



732

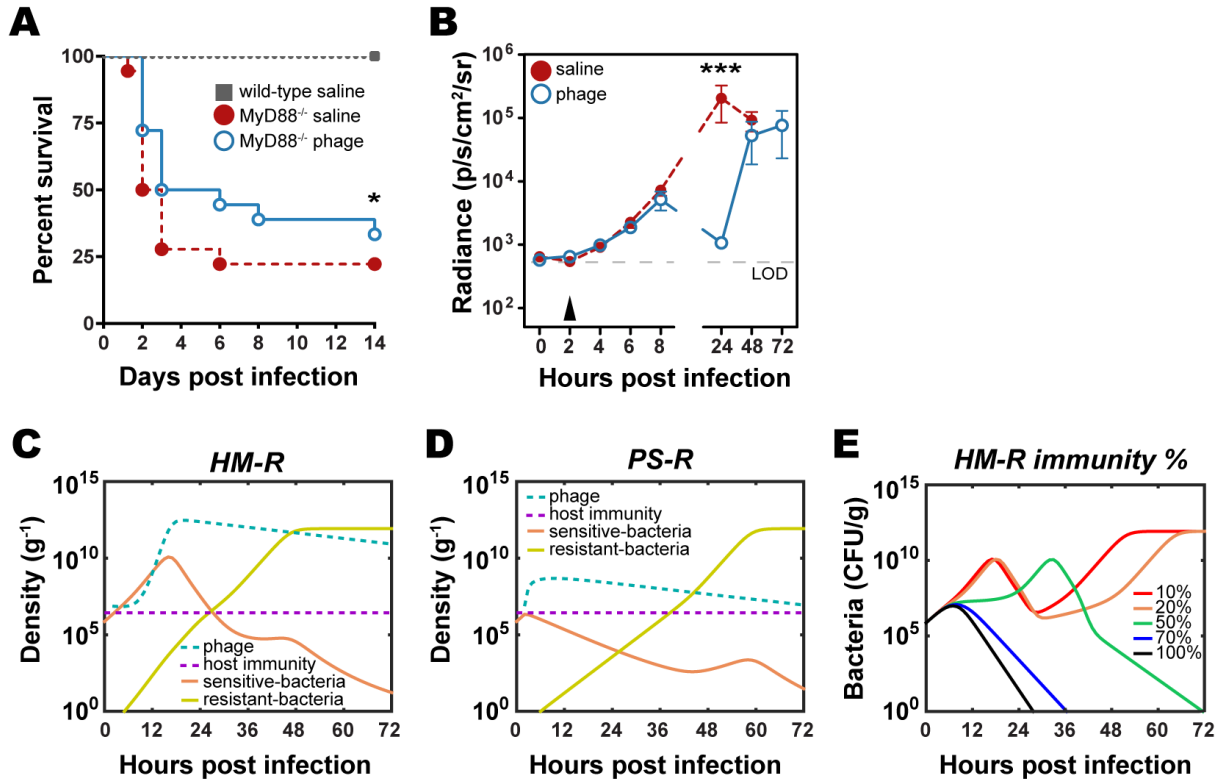
733

734 Figure 2



735

736 Figure 3



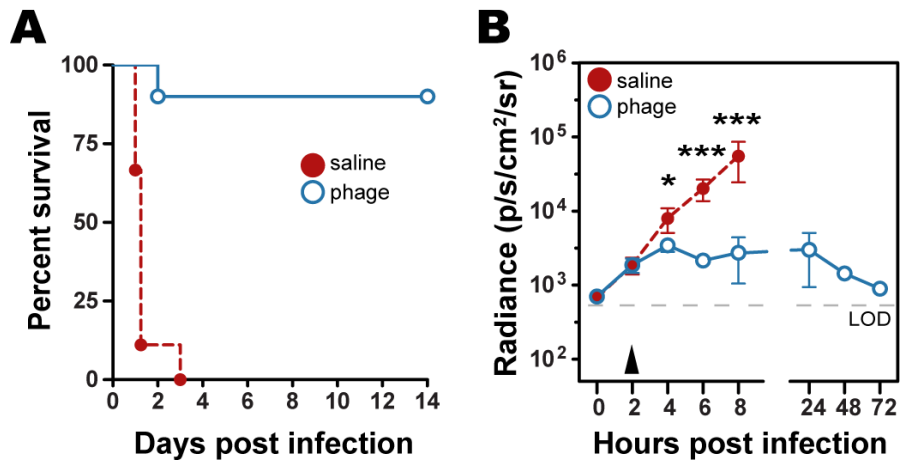
737

738

739

740

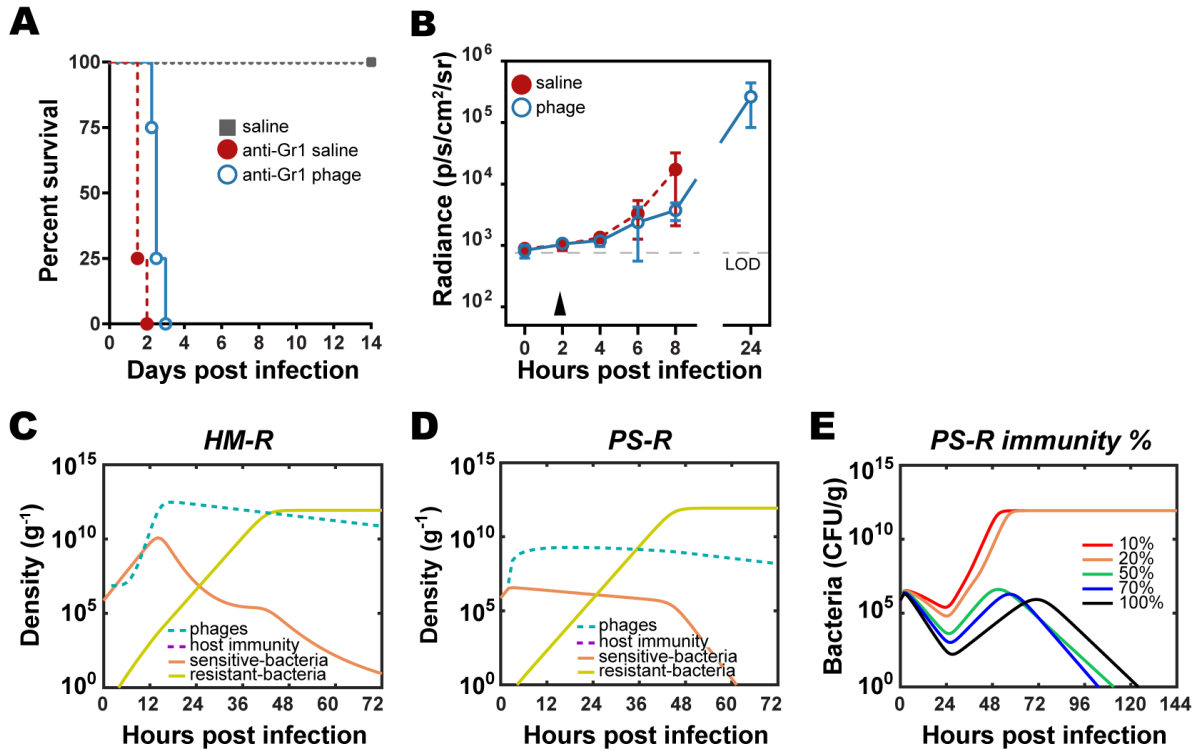
741 Figure 4



742

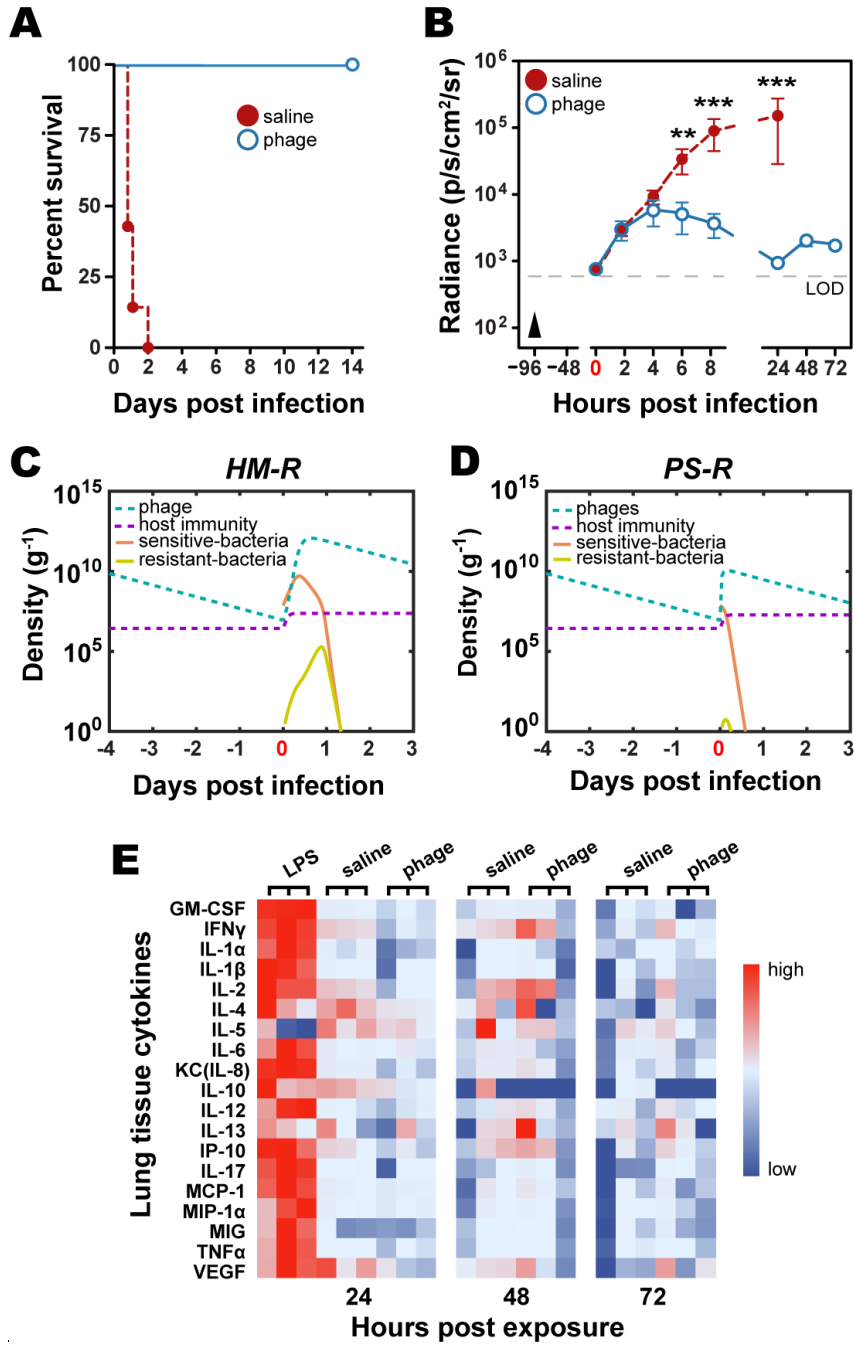
743

744 Figure 5



745

746



748

749

750

751

752 **STAR Methods Text**

753 **CONTACT FOR REAGENT AND RESOURCE SHARING**

754 Further information and requests for resources and reagents should be directed to and will be  
755 fulfilled by the Lead Contact, Laurent Debarbieux (laurent.debarbieux@pasteur.fr)

756

757 **EXPERIMENTAL MODEL AND SUBJECT DETAILS**

758 **Microorganisms**

759 The *P. aeruginosa* PAKlumi strain expressing the *Photorhabdus luminescens luxCDABE* operon  
760 (Moir et al., 2007) was cultured in lysogeny broth (LB) at 37°C. Pseudomonal phage PAK\_P1  
761 (Debarbieux et al., 2010; Henry et al., 2013) was amplified in mid-log growing PAKlumi  
762 overnight after inoculation at the multiplicity of infection (MOI) 0.001. Cell lysate supernatants  
763 containing amplified phages were 0.22 µm filter sterilized and concentrated by ultrafiltration  
764 (Vivaflow 200, Sartorius) in phosphate buffer saline (PBS). Phage PAK\_P1 was purified by two  
765 cesium chloride density gradient centrifugations (Debarbieux et al., 2010), dialyzed in Tris  
766 buffer (10 mM Tris, 150 mM NaCl, pH 7.5) and endotoxin removed by 3 passages through an  
767 EndoTrap HD column (Hyglos, Germany). Phage titer were determined from stocks or lung  
768 tissue homogenates by spotting serial dilutions on seeded lawns of mid-log growing PAKlumi at  
769 OD<sub>600</sub> 0.2. A single phage PAK\_P1 stock stored at 4°C was used for all experiments.

770

771 **Animals and Ethics**

772 Wild-type BALB/c (C), wild-type C57Bl6/J (B6), recombination-activating gene 2 and  
773 interleukin 2-receptor γ- chain double-deficient (Rag2<sup>-/-</sup>Il2rg<sup>-/-</sup>) (Mazurier et al., 1999), and  
774 myeloid differentiation primary response gene 88 (Myd88<sup>-/-</sup>) (Kawai et al., 1999) male and

775 female mice were used between the ages of 8 to 16 weeks. Corresponding groups of mice were  
776 age and gender matched and housed under pathogen-free conditions with *ad libitum* access to  
777 food and water. Animal experiments were conducted in accordance with European directives on  
778 animal protection and welfare, approved by the French Ministry of Education and Research (Ref.  
779 #2012-0018 and #2015-0041) and Institut Pasteur (Ref. #0.565).

780

## 781 **METHOD DETAILS**

### 782 ***In vivo* acute pneumonia mouse model**

783 We used the luminescent *P. aeruginosa* PAKlumi strain and *in vivo* imaging with the IVIS  
784 platform (PerkinElmer), as a noninvasive assessment of acute infection in mouse lungs (Andreu  
785 et al., 2011; Debarbieux et al., 2010; Munder et al., 2014). Subject groups consisted of: (i)  
786 immunocompetent wild-type; (ii) lymphocyte deficient Rag2<sup>-/-</sup>Il2rg<sup>-/-</sup>; (iii) pathogen associated  
787 pattern recognition receptor deficient MyD88<sup>-/-</sup>; and (iv) neutrophil depleted wild-type mouse  
788 strains. Neutrophils were depleted 24h prior to infection by intraperitoneal injection of anti-Gr1  
789 antibody (200 µg; BioXcell) as previously described (Albanesi et al., 2013).

790

791 Mice were infected with intranasally instilled mid-log growing PAKlumi that was washed 3  
792 times in sterile dH<sub>2</sub>O and suspended PBS at an infectious dose of 1.0 x 10<sup>7</sup> colony forming units  
793 (CFU) in 30 µL. We have previously shown that this infectious challenge and route of  
794 administration causes wild-type mouse fatality within approx. 48h (Debarbieux et al., 2010). Due  
795 to the increased susceptibility to infection, Myd88<sup>-/-</sup> and neutrophil depleted mice were  
796 challenged a lower infectious dose of 1.0 x 10<sup>5</sup> CFU PAKlumi. Twenty-four hours after bacterial  
797 challenge, lungs from wild-type mice were aseptically removed, homogenized in PBS and

798 further diluted to obtain calibration data on CFU/photons emitted. Phage resistance was  
799 determined by spotting serial dilutions of fresh phage PAK\_P1 on seeded lawns of 10 isolated  
800 CFUs from treated lung tissue homogenates per *MyD88*<sup>-/-</sup> mouse.

801

## 802 **Curative and prophylactic phage therapies**

803 In wild-type mice, treatment with phage PAK\_P1 was administered intranasally at a curative  
804 dose of  $1.0 \times 10^8$  plaque forming units (PFU; MOI 10) in 30  $\mu$ L PBS at 2h p.i., or at a  
805 prophylactic dose of  $1.0 \times 10^9$  PFU in 30  $\mu$ L PBS 4d prior bacterial challenge. In  
806 immunodeficient mice, treatment with phage PAK\_P1 was administered intranasally at a  
807 curative dose of  $1.0 \times 10^7$  (PFU; MOI 100) in 30  $\mu$ L PBS at 2h p.i. PBS was used as the mock-  
808 treatment control.

809

## 810 **Lung tissue cytokines**

811 Soluble cytokines and chemokines were measured in lung tissue of wild-type mice that received  
812 only intranasally instilled phages at the  $10^9$  PFU in 30  $\mu$ L PBS prophylactic dose. Cytokine  
813 differential expressions were compared to PBS or 10  $\mu$ g LPS from *P. aeruginosa* (Sigma)  
814 controls also administered intranasally. Mouse lungs were harvested, weighed and homogenized  
815 in PBS supplemented with protease inhibitor (cOmplete Ultra Tablets, Roche) with the  
816 gentleMACS Octo Dissociator (Miltenyi Biotec) and centrifuged at 500 rpm to remove large  
817 debris. Cytokines were detected and quantified in lung tissue homogenates using a multiplex  
818 cytokine and chemokine magnetic microsphere-based immunoassay (LMC0006, Life  
819 Technologies) on the Luminex platform and xPONENT software as per the manufacture's  
820 recommendations.

821

## 822 **Mathematical model formulation**

823 The schematic of the model (Fig. 2A) represents a system of nonlinear, coupled differential  
824 equations (Eq. 1-3) that governs the time evolution of the bacterial density  $B$ , phage density  $P$   
825 and immune response intensity .

$$\dot{B} = \overbrace{rB \left(1 - \frac{B}{K_C}\right)}^{\text{Growth}} - \overbrace{BF(P)}^{\text{Lysis}} - \overbrace{\frac{\epsilon IB}{1 + B/K_D}}^{\text{Immune killing}}, \quad 1$$

$$\dot{P} = \overbrace{\beta BF(P)}^{\text{Viral release}} - \overbrace{\omega P}^{\text{Decay}}, \quad 2$$

$$\dot{I} = \overbrace{\alpha I \left(1 - \frac{I}{K_I}\right) \frac{B}{B + K_N}}^{\text{Immune stimulation}}. \quad 3$$

826

827 The parameters  $r$  and  $K_C$  are the maximum growth rate and carrying capacity of the bacteria  
828 respectively. The function  $F(P)$  is the per-capita rate of infection. If the environment is well-  
829 mixed, then the functional form  $F(P) = \phi P$  is linear where  $\phi$  is the adsorption rate (Leung and  
830 Weitz, 2016). The maximum per-capita killing rate of the immune response is given by  $\epsilon$ . When  
831 the bacteria is at high concentration, the immune response is less effective due to the immune  
832 evasion, with  $K_D$  being the bacterial density at which the immune response is half as effective.  
833 The phage replicate with an effective burst size of  $\beta$  and decay at a rate of  $\omega$ . The immune  
834 response is stimulated by the presence of bacteria with a maximum activation rate  $\alpha$  until it  
835 reaches the maximum capacity  $K_I$ .  $K_N$  is the bacterial density at which the immune intensity  
836 growth rate is half its maximum.

837

838 Preliminary *in silico* analysis of this model found that if the environment is well-mixed, then  
839 inclusion of the linear form  $F(P) = \phi P$  leads to extremely rapid elimination of bacteria using

840 parameters corresponding to *in vivo* phage treatment in immunocompetent host (Fig. S2A). The  
841 rapid bacteria elimination is apparent even in the absence of innate immunity (Fig. S2B),  
842 suggesting that the linear model overestimates the rate of phage killing. We modify the  
843 functional form of  $F(P)$  to account for spatial heterogeneity in the lungs (which we term the  
844 heterogeneous mixing (*HM*) model) and the effects of saturation of phage infection at high phage  
845 dose (which we term the phage saturation (*PS*) model); see text for more details.

846

847 In the *HM* model, spatial heterogeneity is modeled by a power-law dependence of the phage  
848 infection rate (Bansal et al., 2007; Liu et al., 1987; Roy and Pascual, 2006)

$$F(P) = \tilde{\phi}P^\gamma \quad 4$$

849

850 where  $\tilde{\phi}$  is the nonlinear phage adsorption rate and  $\gamma$  is the power-law exponent. In the *PS*  
851 model, saturation effects are modeled by the saturating Hill function

$$F(P) = \frac{\phi P}{1 + P/P_C} \quad 5$$

852

853 where  $P_C$  is the phage concentration at which the phage infection rate is half-saturated and the  
854 expression reduces to the linear form when  $P \ll P_C$ . The phage infection rates as functions of the  
855 phage density for the well-mixed linear model ( $F(P) = \phi P$ ), *HM* model, and *PS* model are  
856 shown in Figs. S2C, S2D and S2H, respectively. The well-mixed linear model likely  
857 overestimates the phage infection rate, reaching about  $40 \text{ h}^{-1}$  at the initial phage dose for curative  
858 treatment ( $7.4 \times 10^8$  PFU). In contrast, both the *HM* model and *PS* model result in lower  
859 estimates for the phage infection rate more likely to be biologically relevant.

860

861 We also extended the model to include emergence of phage resistance in the bacterial

862 population, which was experimentally observed in the Myd88 deficient mice. In this phage  
863 resistance model, the bacterial population consists of a phage-sensitive subpopulation  $S$  and  
864 phage-resistant subpopulation  $R$  (Fig. 2D). The phage-sensitive bacteria are infected and lysed  
865 by the phage, while the phage-resistant bacteria do not interact with the phage (Eq. 6-8). Similar  
866 to the model without resistance, infection of sensitive bacteria by phage is either subjected to  
867 heterogeneous mixing (Eq. 4) or saturation (Eq. 5), which we term as the heterogeneous mixing-  
868 resistance ( $HM-R$ ) model and phage saturation-resistance ( $PS-R$ ) model respectively. Phage  
869 resistance is acquired by phage-sensitive bacteria through mutation with a fixed probability  $\mu$  per  
870 cellular division (see Eq. 6-7) (Luria and Delbruck, 1943). Both phage-sensitive and phage-  
871 resistant bacteria are killed by the immune response (Eq. 6-7) and stimulate immune activation  
872 (Eq. 9). In general, the phage-resistant strain can have a different maximum growth rate  $r'$  (Eq.  
873 7) from the phage-sensitive strain. For example, phage resistance can come with evolutionary  
874 trade-offs as reflected by a reduction in growth rate (Bohannan et al., 2002; Weitz, 2015).

$$\dot{S} = \overbrace{rS \left(1 - \frac{S+R}{K_C}\right)}^{\text{Growth}} \overbrace{(1-\mu)}^{\text{Mutation}} - \overbrace{SF(P)}^{\text{Lysis}} - \overbrace{\frac{\epsilon IS}{1 + (S+R)/K_D}}^{\text{Immune killing}}, \quad 6$$

$$\dot{R} = \overbrace{r'R \left(1 - \frac{S+R}{K_C}\right)}^{\text{Growth}} + \overbrace{\mu rS \left(1 - \frac{S+R}{K_C}\right)}^{\text{Mutation}} - \overbrace{\frac{\epsilon IR}{1 + (S+R)/K_D}}^{\text{Immune killing}}, \quad 7$$

$$\dot{P} = \overbrace{\beta SF(P)}^{\text{Viral release}} - \overbrace{\omega P}^{\text{Decay}}, \quad 8$$

$$\dot{I} = \overbrace{\alpha I \left(1 - \frac{I}{K_I}\right) \left(\frac{S+R}{S+R+K_N}\right)}^{\text{Immune stimulation}}. \quad 9$$

875

## 876 Parameter estimation

877 See Table S1 for *in silico* model parameters. The life history traits of the bacteria and phage are  
878 obtained from empirical values from a *P. aeruginosa* murine pneumonia model (Drusano et al.,

879 2011) and *P. aeruginosa* strain PAKlumi and phage PAK\_P1 used in this study. In wild-type  
880 mice, we measured the bacterial density 24h post infection ( $2.4 \times 10^9$  CFU/g, see results section  
881 for details) and used it to estimate the carrying capacity  $K_C$  in hosts with healthy immune  
882 responses. The decay rate  $\omega$  of phage is estimated from the fitted phage half-life. The immune  
883 response intensity is taken to be the neutrophil density in the lungs, given the present  
884 identification of neutrophils as critical for therapeutic efficacy. Therefore the killing rate  
885 parameter of the immune response  $\varepsilon$  is estimated from the maximum killing rate of neutrophils  
886 (Li et al., 2002).

887

888 For the immunocompetent mice, the maximum activation rate of immune response  $\alpha$ , initial  
889 immune response  $I_0$  and maximum immune response  $K_I$  are estimated from fitting of neutrophil  
890 recruitment data in the lungs (Reutershan et al., 2005). For mice that are Myd88 deficient, their  
891 innate immune activation is disrupted and we model that by reducing the maximum (activated)  
892 immune response  $K_I$  to the level of the initial immune response  $I_0$ . We further investigate the  
893 effects of restoring intermediate levels of immune activation by setting

$$K_I \rightarrow I_0 + s(K_I - I_0) \quad 10$$

894

895 where  $s$  is a scaling parameter from 0% (no immune activation) to 100% (normal immune  
896 activation).

897

898 For mice with neutrophils depleted by anti-Gr-1 antibodies, we assume negligible primary innate  
899 immunity and set  $I = 0$ . We further model intermediate levels of neutrophil depletion by setting  
900 the immune intensity as a fixed percentage of the normal immune intensity, *i.e.*

$$I \rightarrow s'I$$

901  
902 where  $s'$  is a parameter that goes from 0% (complete lack of innate immunity) to 100% (normal  
903 innate immunity). The bacteria concentration  $K_D$  at which immune response is half as effective is  
904 assumed to be close to the bacterial inoculum that leads to a lethal infection ( $5.5 \times 10^6$   
905 CFU/lung). The bacterial density  $K_N$  at which immune growth rate is half its maximum is  
906 obtained from *in vitro* data of the response of a pathogen recognition receptor (i.e. Toll-like  
907 receptor 5) to the *P. aeruginosa* strain PAK (Zhang et al., 2005). Initial bacterial load and phage  
908 concentrations are set by the corresponding doses used in the experiments.

909  
910 We select the parameters of the nonlinear phage infection rates in the *HM* and *PS* model by first  
911 performing a sensitivity analysis. As a reference point, the linear adsorption rate for the phage  
912 PAK\_P1 is about  $5.4 \times 10^{-8}$  g/h PFU measured at an MOI of 0.001. For the *HM* model, we  
913 expect the nonlinear adsorption rate  $\tilde{\phi}$  would be close to this value when  $\gamma \rightarrow 1$ . We vary both  $\tilde{\phi}$   
914 and the power law exponent  $\gamma$  and measure the minimum bacterial density reached in a  
915 simulation within 72h post infection in the absence and presence of innate immune response  
916 (Figs. S2E and 2F, respectively). When  $\tilde{\phi}$  and  $\gamma$  are increased, the minimum bacterial density  
917 reduces until it reaches the point of extinction, *i.e.*, when bacterial density is below 1 CFU/g. The  
918 parameters  $\tilde{\phi}$  and  $\gamma$  are chosen to be within the phage-immune synergistic regime, where the  
919 bacterial population only becomes extinct in the presence of immune response (Fig. S2G).  
920 Outside the phage-immune synergistic regime, the phage either eliminates the bacteria on its own  
921 (phage sufficient regime), or fail to do so even when combined with immune response (phage-  
922 immune insufficient regime). A similar analysis is conducted for the *PS* model by varying the  
923 adsorption rate  $\phi$  and half-saturation phage concentration  $P_C$  in the absence and presence of

924 innate immune response (Figs. S2I and S2J, respectively). The values of  $\phi$  and  $P_C$  are chosen  
925 accordingly to be within the phage-immune synergistic regime (Fig S2K).

926

927 For the phage resistance model, the probability  $\mu$  of producing a phage-resistant mutant per  
928 cellular division is estimated from *in vitro* experimental measurements (Luria and Delbruck,  
929 1943). We assume a moderate trade-off between phage resistance and growth rate (Bohannan et  
930 al., 2002; Weitz, 2015) with the maximum growth rate of the resistant strain 10% lower than its  
931 phage-sensitive counterpart.

932

### 933 **Simulation of mathematical models**

934 The *in silico* model equations in Eq. 1-3 and Eq. 6-9 are numerically integrated using ODE45 in  
935 MATLAB to obtain the bacteria, phage and immune response time series. Bacteria and phage are  
936 assumed to become extinct in the mice lung when their population densities drop below a  
937 threshold of  $1 \text{ g}^{-1}$ .

938

## 939 **QUANTIFICATION AND STATISTICAL ANALYSIS**

### 940 **Statistical analysis**

941 Statistical analyses were conducted with Prism 5 software (GraphPad). Photon emissions were  
942 log10 transformed prior to analysis by the Mann Whitney or the two-way ANOVA, followed by  
943 Bonferroni post-tests. Log-rank (Mantel-Cox) test compared survival curves and Welches t-test  
944 compared differential expression of cytokines in lung tissue homogenates.  $p < 0.05$  was  
945 considered statistically significant.

946

947 **DATA AND SOFTWARE AVAILABILITY**

948 The source code for the mathematical models is included in the supplemental files as Data S1

949 and will also be deposited in Github.

950